Materials Chemistry and Physics 192 (2017) 41–47

Contents lists available at ScienceDirect

Materials Chemistry and Physics

journal homepage: www.elsevier.com/locate/matchemphys

Electrical, thermoelectrical and magnetic properties of approximately 20-nm Ni-Co-O nanoparticles and investigation of their conduction phenomena

E.M.M. Ibrahim [a], Ahmed M. Abu-Dief [b, c], A. Elshafaie [a, *], A.M. Ahmed [a]

[a] Physics Department, Faculty of Science, Sohag University, Sohag, 82524, Egypt
[b] Chemistry Department, Faculty of Science, Sohag University, Sohag, 82524, Egypt
[c] Departamento de Quimica Organicae Inorganica, Faculad de Quimica, Universdad de Oviedo, 33006, Oviedo, Spain

HIGHLIGHTS

- Presents novel method for synthesis Ni-Co-O nanoparticles.
- This article gives a significant understanding on the conduction mechanism of Ni-Co-O nanoparticles.
- Present a novel comprehensive study on the type of carriers which governs the conduction mechanism.
- The magnetic phase either antiferromagnetic or paramagnetic of all samples also has been studied.

ARTICLE INFO

Article history:
Received 17 May 2016
Received in revised form
21 December 2016
Accepted 16 January 2017
Available online 20 January 2017

Keywords:
Ni-Co oxide nanoparticles
Electrical properties
Magnetic properties
Spinel structure

ABSTRACT

Understanding the properties of semiconductor nanostructures is important for developing their practical applications in the nanodevices. Although the electrical properties of spinel oxides containing Ni and Co have been studied extensively over the last decades, there is still a significant disagreement on their electrical conduction mechanisms and the distribution of the various charge states of Co and Ni in the octahedral and tetrahedral sites of the spinel crystal lattice. In this study, Co_3O_4, NiO, and mixed Ni-Co oxide nanoparticles (NPs) of ~20 nm are synthesized by co-precipitation method. The mechanism of the electrical conduction in the Co_3O_4 and Ni-Co oxides NPs is due to the hopping process in the octahedral site or between the octahedral and tetrahedral sites while in the NiO NPs, the large polarons conduction mechanism dominates. The thermoelectric power measurements confirm that the Ni-Co oxides NPs are non-degenerate semiconductors and the diffusion mechanism is the dominant component of the Seebeck coefficient. In contrast, the Co_3O_4 NPs show degenerate features with Fermi energy 0.054 eV. The NiO NPs exhibit a transition from non-degenerate to degenerate state. The magnetic measurements reveal an antiferromagnetic-paramagnetic transition at Néel transition temperature. The results are helpful to understanding the fundamental characteristics of the NPs under study.

1. Introduction

Semiconductor nanostructures have attracted significant interest in the past few years because they initiate new generation of functional nanodevices, such as solar cells, photodetectors, light emitting diodes, field-effect transistors and sensors [1–4]. Mixed cobalt-nickel oxides are promising transition metal oxide semiconductors. They have spinel structure (octahedral and tetrahedral) AB_2O_4 in which Ni^{2+} and/or Co^{2+} occupies the octahedral sites while Co^{3+} distributes over both octahedral and tetrahedral sites [5,6]. These spinel oxides have shown exceptional ability to serve as an oxygen evolution electrode and have been studied quite extensively by electrochemical methods for this purpose [1,2]. Also, the exquisite point is that the Ni-Co oxides can be utilized as electrode materials in sodium and sodium ion cells as well as electrocatalyst in advanced alkaline water electrolyzer due to their high electrical conductivity and desirable optical properties in the infrared regions [1]. Recently, Hu et al. enhanced the optoelectronic properties of the Ni-Co oxide nanofilms in high-frequency

* Corresponding author.
E-mail address: Shafaie_phy@yahoo.com (A. Elshafaie).

http://dx.doi.org/10.1016/j.matchemphys.2017.01.054
0254-0584/

photodetector device where the nanofilms showed good sensitivity and ultrafast response time of several microsecond [7,8]. It has to be highlighted that, study of the electrical transport properties of the Ni-Co nanoparticles is crucial to promote their practical applications in high-performance nanodevices, where, predictable and controllable conductance is necessary to many nanoscale electrical applications. Indeed, although the electrical properties of bulk spinel oxides containing Ni and Co have been studied extensively over the last decades [9–13], there is still significant disagreement on two main issues, first: the electrical conduction mechanism and second: the internal structure particularly, the distribution of the various charge states of Co and Ni in the octahedral and tetrahedral sites of the spinel crystal lattice. Besides, producing these materials in the nanoscale has been accompanied by changes in their properties which need further study and investigations. Commonly, it is accepted that Co_3O_4 is a p-type spinel material. However, there is a disagreement on whether conduction is intrinsic or due to impurity doping and on how mobile the holes are [9,10,12,14,15]. There are many opinions suggest that the conduction in the Co_3O_4 is due to the small polaron hopping of holes particularly when the lattice contains specific contents of defects [10,15,16]. But others suggest that common charge carriers hopping between the divalent cations (Co^{2+}) and the trivalent cations (Co^{3+}) located in the tetrahedral and octahedral sites of the spinel structure is responsible for the conduction [10–12,15,17]. The situation of Ni-Co oxide is more complicated because the spinel system may have four ions instead of two because Ni may exist in +3 and +2 oxidation states. Although it is generally accepted that Ni ions prefer to occupy octahedral sites in the spinel system, the distribution of Co ions and the charge state of the Ni have been widely debated. Therefore, this work describes an experimental approach to developing our understanding of the electrical transport as well as the magnetic properties of the Ni-Co oxides nanoparticles. To achieve the desired goal, the strategy is based on studying the evolution occurs in the properties of the Co_3O_4(0% Ni) nanoparticles by increasing the Ni toward the synthesis of the NiO (100%Ni) nanoparticles.

2. Experimental procedure

2.1. Synthesis of the nanoparticles

2.1.1. Materials

To synthesize the Co and Ni oxide nanoparticles (Ni-Co oxides NPs), the $Ni(NO_3)_2{\cdot}4H_2O$ and $Co(NO_3)_3{\cdot}4H_2O$ (Sigma-Aldrich) compounds were used as the nickel and cobalt precursors while NaOH (pellets, 98%, Alfa Aesar) acted as a precipitant. All reagents were of analytical grade and used without further purification. All solutions were prepared with bidistilled water.

2.1.2. Procedures

To prepare the Ni-Co oxides NPs, in the desired Ni ratios (Ni = 0, 20, 40, 60 and 100%), stoichiometric molar amounts of Nickel nitrate Ni(NO3)2·4H2O and Cobalt nitrate Co(NO3)3·4H2O were each dissolved in 20 ml of distilled water to form clear solutions which were mixed together. The mixtures were stirred with a magnetic stirrer until the reactants were dissolved completely. During the stirring processes, 5 ml of PEG-400 was added dropwise to the solutions of the mixtures to serve as a surfactant that covers the NPs and prevents their agglomeration. The obtained solutions were stirred for additional 1/2 h to guarantee the complete mixing of the PEG with the reactants. After that, the pH of the solutions was adjusted to be 12. This was achieved by adding 2 M NaOH drop-by-drop with stirring. After continuous stirring at 500 rpm for 1 h, homogeneous solutions containing hydroxide precipitates of the reactants were obtained. The obtained products were centrifuged and washed several times with water, absolute ethanol and acetone. Then, the obtained samples were dried in an oven at 120 °C for 6 h. Finally, the dried samples were calcined at 500 °C for 3 h with heating rate 10 °C/min and then cooled gradually to the room temperature. The obtained solid phase samples were grinded thoroughly in an agate mortar and were used for all the measurements.

2.1.3. Instruments

The pH of the solution of the prepared nanoparticles was adjusted by a single electrode pH-meter (Denver Instrument Co., USA). The structure of the sample was investigated by the x-ray powder diffraction (XRPD) technique, being the x-ray patterns from 5° to 80° at 2θ with a step of 0.05° and a counting time of 2.5 s/step collected by a Philips X'Pert PRO MPD (PANalytical, The Netherlands) using graphite-monochromatized Cu-Ká radiation (ë = 1.54184 Å) operating at 45 kV and 40 mA. The instrument resolution (programmable divergent slits) was determined using LaB6 standard reference material (SRM 660a) provided by National Institute of Standards and Technology (NIST), commonly used for calibrating line position and line shape in powder diffractometers. The morphology of the prepared samples was studied by field-emission scanning electron microscopy (FE-SEM) JSM-6100 microscope (JEOL, Japan) with an acceleration voltage of 30 kV. The chemical composition of the synthesized nanostructures was also analyzed using the energy dispersive analysis of x-ray (EDAX) unit attached to the FE-SEM. Transmission electron microscopy (TEM) studies were performed using a JEOL JEM-2100F transmission electron microscope operated at an accelerating voltage of 200 kV. The samples for TEM were dispersed in ethanol, sonicated and sprayed on a carbon-coated copper grid and then allowed to air-dry, finally, Gatan SOLARUS 950 was used before observation. The electrical properties were studied by measuring the electrical conductivity as a function of temperature using a so-called two-prope method in the temperature range 373–593 K. The temperature dependence of Seebeck coefficient was determined in order to study the thermoelectric properties of the nanoparticles. The measurements were carried out within a temperature range 93–323 K using specially made sample holder. The electrical conductivity and Seebeck coefficient measurements were carried out in a vacuum of 10^{-3} mmHg which was found to contribute much to the thermal stability during the measurements. The temperature of the sample and the temperature gradient in the thermoelectric measurement were sensed by standard copper-Constantan thermocouples. The AC magnetic measurements were studied through measuring the variation of the susceptibility with the temperature in the temperature range 93–400 K using the Bartington Instrument MS2C system where the equipment located in a place away from the potential sources to avoid the electrical noise. we must also take into considerations that a type T thermocouple connected at low temperature and a type S connected at high temperature and the powder sample fixed in ceramic cylindrical pillboxes.

3. Results and discussions

3.1. Structural characterization

The XRD patterns presented in Fig. 1a and e for Co_3O_4 and NiO nanoparticles (NPs) indicate that all the diffraction peaks are assigned to the Co_3O_4 (JCPDS card 43-1003) and NiO (JCPDS 47-1049) phases, respectively. No other peaks for impurities of other Co or Ni-based compounds were detected. For Ni-Co oxides NPs, the XRD patterns (Fig. 1b–d) confirm that the peaks can be assigned to $NiCo_2O_4$ and/or Co_3O_4 phases. Noteworthy, discrimination between the $NiCo_2O_4$ and Co_3O_4 by XRD is quite difficult because they

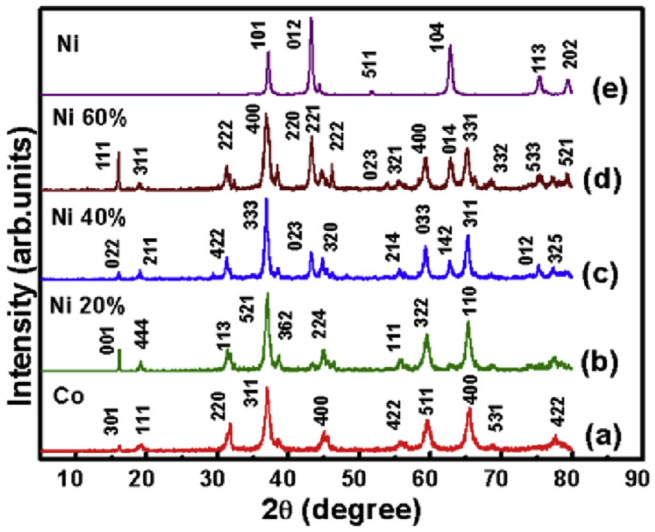

Fig. 1. XRD patterns for Co_3O_4, NiO, and Ni-Co oxides NPs.

have similar spinel structure with a small difference in lattice parameter ($NiCo_2O_4$: 8.110 Å and Co_3O_4: 8.084 Å). However, the peaks shift to lower 2θ compared to the pattern *a* (of the pure Co_3O_4) confirm the incorporation of the Ni ions in the Co_3O_4 lattice. The average crystallite size D_{XRD} was calculated using the Scherer formula $D_{XRD} = 0.89\lambda/\beta\cos\theta$ [5] where, β is the angular line width at half maximum intensity and θ is the Bragg's angle for the actual peak. The D_{XRD} values are tabulated in Table 1 and shows that the average size of the Co_3O_4 nanocrystallites has the largest value and decreases with the increase of the Ni content. Noteworthy, the crystallites of the Ni-Co oxides samples have nearly the same size. The broadening of the peaks suggests a crystalline nature of the samples and could also arise from the micro-straining of the crystal structures due to defects like dislocations, twinning etc. These types of defects are believed to associate with the chemically synthesized nanocrystals as they grow spontaneously during the chemical reaction and hence the chemical ligands get negligible time to diffuse to the energetically favorable sites. They could also arise due to lack of sufficient energy needed by an atom to move to a proper site forming the crystallite [18].

The morphology of the samples was investigated by the field emission scanning electron microscope (FESEM). It is important to say that, no significant difference in the overall morphology of whether the pure Co_3O_4, NiO or Ni-Co oxide NPs was observed. Consequently, only a SEM image of the NiO NPs has been presented in Fig. 2a as an example. The SEM investigation confirms that the materials consist of NPs in nearly spherical shape. The EDX analyses indicate that all the compositions have the desired stoichiometric ratios as seen in Fig. 2b for NiO sample as an example. The morphology of the NPs in all samples is highlighted by the HRTEM images in Fig. 2c–g. In general, the images confirm the nano-sized crystallite structure of the particles. To be specific, Fig. 2c clearly implies good crystallinity of the Co_3O_4 crystallites by an appearance of fringes of the lattice planes (marked in the figure by white parallel lines). Noteworthy, the same results were obtained from the HRTEM images (not included here) of the other samples where the internal structure could be clearly identified. In addition, the size and size distribution of the NPs were extracted from the TEM images and the obtained results of this analysis have been illustrated in the histograms depicted as insets in Fig. 2d–g. The average nanoparticle size D_{TEM} of Co_3O_4 is 24 nm with size distribution ranges from 14 to 34 nm. The D_{TEM} values decrease with the addition of Ni and the size distributions become narrower (see Table 1). Note that, the D_{TEM} values are slightly higher than the crystallites size D_{XRD} values determined from the XRD results because the nanoparticle is an aggregation of more than one nanocrystallite [19].

3.2. Electrical properties

The electrical behavior of the NPs was studied by measuring the dc conductivity σ as a function of temperature T. The σ-T plots are depicted in Fig. 3a. The results reveal that the materials are characterized by semiconductor behavior i.e. by increasing the temperature, more and more charge carriers can overcome the energy barrier and participate in the electrical conduction. Noteworthy, a low DC electrical conductivity in the order of fractions of $(pico\text{-}ohm.cm)^{-1}$ was found for the samples below the room temperature and it was not possible to be exactly determined due to the measurement limitations.

The σ-T plots could be relatively described by the Arrhenius relation [20]:

$$\sigma = \sigma_0 \, exp\left(\frac{-\Delta E}{K_B T}\right) \quad (1)$$

where, σ_0 is the conductivity at room temperature, K_B is the Boltzmann constant ΔE is the activation energy and T is the absolute temperature. The linear behavior of the ln(σ) vs. 1000/T plots depicted in Fig. 3b confirms the thermally activated conduction.

of the materials. The activation energy ΔE were calculated and tabulated in Table 1. Noteworthy, to promote the intrinsic conduction in the normal semiconductor, i.e. transfer of the electrons from the filled valence band to the empty conduction band, energy larger than 1 eV is needed [6,21] which means that the obtained ΔE values are too small to support the intrinsic conduction in our NPs. This situation confirms that the band conduction mechanisms omitted at least within the temperature range of measurements for the materials at hand. On the other hand, the carriers concentration for the NPs were calculated using the formula $n = Nexp(-Se/K_B)$ where S is the Seebeck coefficient and e is the electron charge and N is the density of states or the concentration of the electronic levels involved in the conduction process and calculated from the formula: $N(E) = \left(\frac{8\pi\sqrt{2}}{h^3}\right)(m^{*3/2})\sqrt{(\Delta E)}$ where h is the Planck's constant and m^* is the effective mass [22]. These formulas allowed

Table 1
Estimated Parameters of Co_3O_4, NiO and Ni-Co oxides NPs.

Metal oxide	D_{XRD} (nm)	D_{TEM} (nm)	ΔE (eV)	n/(cm^{-3})	ΔE_A (eV)	T_N (K)	μ_p (B.M.)
Co_3O_4	11.3 ± 0.1	24	0.027	1.8×10^{22}	0.072	228	183.4
Ni 20%	10.8 ± 0.05	16	0.087	5.8×10^{22}	0.077	188	261.2
Ni 40%	10.7 ± 0.03	14	0.095	6.3×10^{22}	0.13	173	277.3
Ni 60%	10.6 ± 0.03	13	0.099	6.6×10^{22}	0.14	163	298.2
NiO	6.57 ± 0.09	18	0.049	3.2×10^{22}	0.092	213	231.5

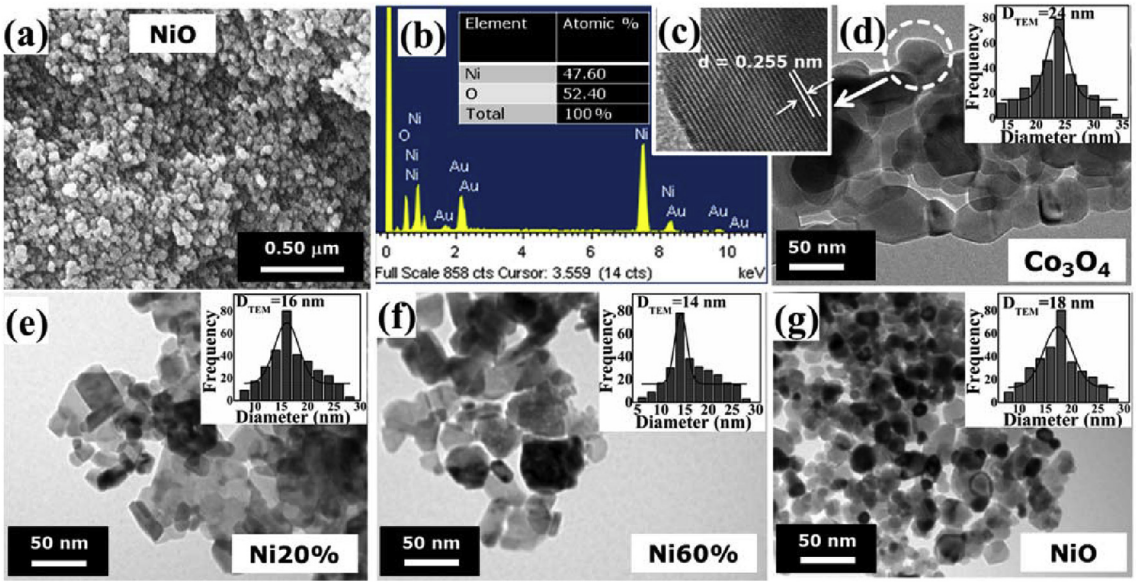

Fig. 2. a) & b) FESEM image and EDX spectrum of the NiO NPs, respectively, c) HRTEM image of the Co3O4NPs, d–g) TEM images of the Co_3O_4, NoO, and Ni-Co oxides NPs (the insets are the corresponding NPs size-distribution histograms).

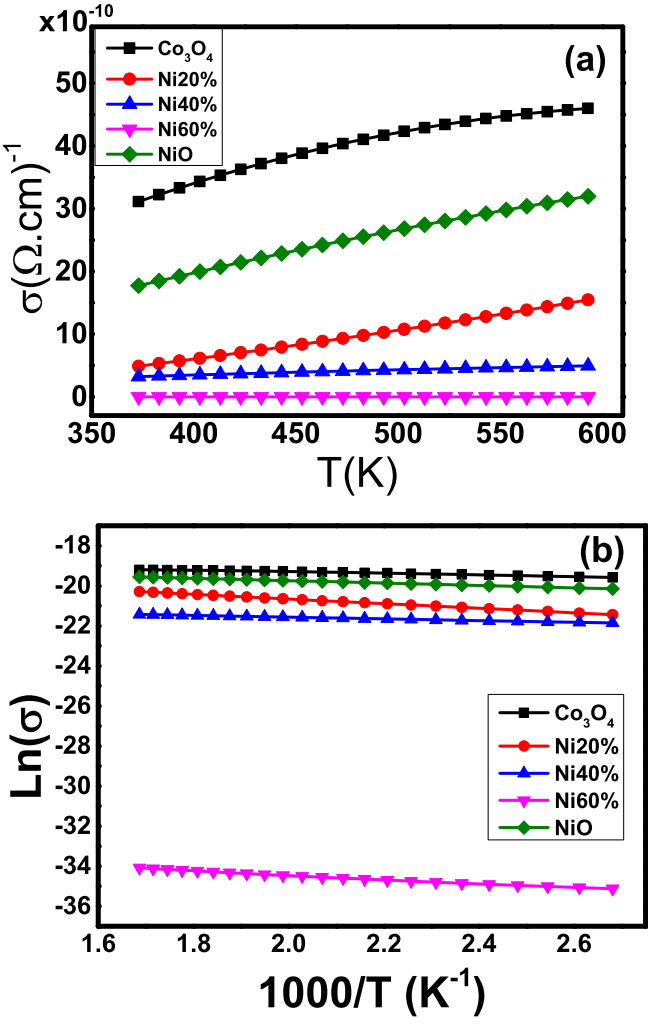

Fig. 3. a) The electrical conductivity s vs. temperature, b) Ln(σ) vs. 1000/T plots of the Co_3O_4, NiO and Ni-Co oxides NPs.

calculating the drift mobility μ_d using the equation $\mu_d = \sigma/ne$ [21]. The μ_d *vs.* T plots presented in Fig. 4 reveal that the μ_d is temperature dependent and possess very small values compared to those characterizing the band conduction mechanism which are additional evidences for omitting of the band conduction mechanism in the NPs.

To investigate the scenario of the conduction mechanism of the NPs under study, their structure should be taken into deep consideration. The Co_3O_4 and Ni-Co oxides crystallize in spinel cubic structure (space group *Fd*3*m*) as a combination of two interpenetrating sub-lattices (octahedral and tetrahedral) in which Ni^{2+} and/or Co^{2+} occupies the octahedral sites while Co^{3+} distributes over both octahedral and tetrahedral sites. At these sites, the crystal fields split five degenerate atomic d orbitals into two groups leading to three unpaired electrons on Ni^{2+} and/or Co^{2+} while the d electrons of Co^{3+} are paired. Because of this scenario of the electronic structure, the concept of electron or polaron hopping can be invoked. Consequently, increasing the conductivity with the temperature (semiconductor regime) is attributed to that the

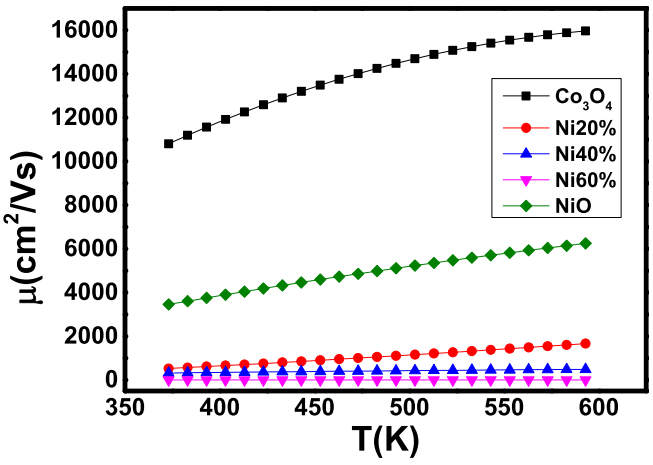

Fig. 4. Charge mobility of the Co_3O_4, NiO, and Ni-Co oxides NPs.

elevated temperatures provide enough energy for charge carriers to hop among sites or even from defects involving singly charged oxygen ions. These oxygen defects could add additional charge carriers to increase conductivity [6].

The energy anticipated in the hopping process whether between the Ni^{2+} and/or Co^{2+} and the Co^{3+} in the octahedral site or between the octahedral and tetrahedral sites can be estimated from the following formula [23]:

$$\sigma = \left(\frac{const.}{T}\right) e^{-\Delta E_A / K_B T} \quad (2)$$

where ΔE_A is the energy consumed in the conduction (the energy required to transfer the charge carriers between the two states, hopping energy, in addition to a part of energy required for the carrier mobility) and K_B is the Boltzmann's constant. The ln(σ T) vs, 1000/T plots, illustrated in Fig. 5, allows to calculate the values of ΔE_A and the data are tabulated in Table 1.

In the NiO NPs, the scenario of the conduction mechanism is significantly different and can be attributed to competing of two contributions, specifically, the small polarons in the 3d of Ni^{2+} and the large polarons in the 2p band of O^{2-}. It has been reported that, the small polarons conduct only by means of thermally activated hopping at temperatures above 100 K while a band like conduction due to large polarons in the 2p band of O^{2-} dominates at temperature higher than 200 K [24,25]. Our results indicate that the large polarons conduction dominates and the activation energy ΔE_A was calculated from the linear fit shown in Fig. 5. ΔE_A has a value of 0.092 eV which is relatively low in comparison to the values published in other literature; for example Makhlouf et al. [26] reported activation energies of 0.36 and 0.5 eV for samples of average particle size 28.6 and 100 nm, respectively. The difference in the activation energies may be attributed to the differences in the particle size and the oxygen content as well as a minor contribution of the small polarons to the conduction.

The results presented in Fig. 3 reveal decreasing in conductivity with increasing the amount of nickel in the Ni-Co oxides NPs over the whole temperature range of measurements. Similar behavior was reported by Windisch Jr. et al. [9] for sputter-deposited and solution-deposited Ni-Co oxides thin films. Also, Roffi et al. [27] reported similar results indicating that substitution of homovalent Co^{2+} by Ni^{+2} may not result in any carriers generation while two electrons are generated for every two trivalent cobalt ions substituted by nickel in the lattice and thus the electrical conductivity decreases as the Ni content increases in the Ni-Co oxide materials. On the other side, another reason can be taken in consideration which is the increase of the polaron hopping conduction contribution on the expense of the electron hopping conduction as the Ni content increases. The Polaron hopping is a relatively slower process because a polaron is a combination of a charge carrier and a lattice strain, both of which move during the electrical conduction. It is well known that the conductivity is the product of polaron density, mobility, and an electron's charge. In a polaron hopping system, conductivity is regulated by the polaron density because of the hopping mobility is low [26]. Another explanatory about this point is the increase of the grain boundary scattering due to the decrease of the NPs size as the Ni content increases in the compositions as was shown from the aforementioned results of the XRD and HRTEM investigations.

3.2.1. Thermoelectric power

Thermoelectric power study at low temperature may provide crucial information about the features of the materials which could not be obtained by the electrical measurements because of the high resistance of the materials.

Seebeck coefficient of the NPs under study as a function of temperature are given in Fig. 6. It is well known that Co_3O_4, NiO and their mixed oxides act as a P-type semiconductor that the majority carriers are holes [28,29]. This truth is confirmed also from our results where the Seebeck coefficient values over the whole temperature range of measurements (93–323 K) are positive. The Seebeck coefficients of Ni-Co oxides NPs ($S_{(Ni\text{-}Co\ oxides)}$) were found to decrease with increasing the temperature showing a typical feature of non-degenerate semiconductors. $S_{(Ni\text{-}Co\ oxides)}$ is expected to be generally composed of three contributions; first: a diffusion contribution (S_d), second: a phonon drag contribution (S_g) (although the experimental data are not enough to estimate accurately the phonon drag component, it is expected to be secondary compared to S_d because of alloying elements) and third: a variable range hopping contribution (S_{VRH}) varies as $S_{VRH} \sim T^{1/2}$ which is mainly effective at lower temperatures [26] that is its contribution is expected to be very small to be considered here. On the other hand, considering the non-degenerate nature of the Ni-Co oxides NPs, the S_d can be represented by the following formula [28].

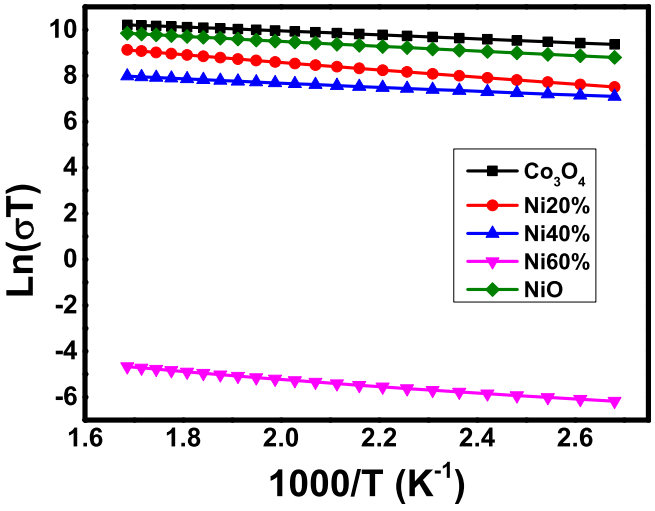

Fig. 5. Ln(σT) vs. 1000/T of the Co_3O_4, NiO and Ni-Co oxides NPs.

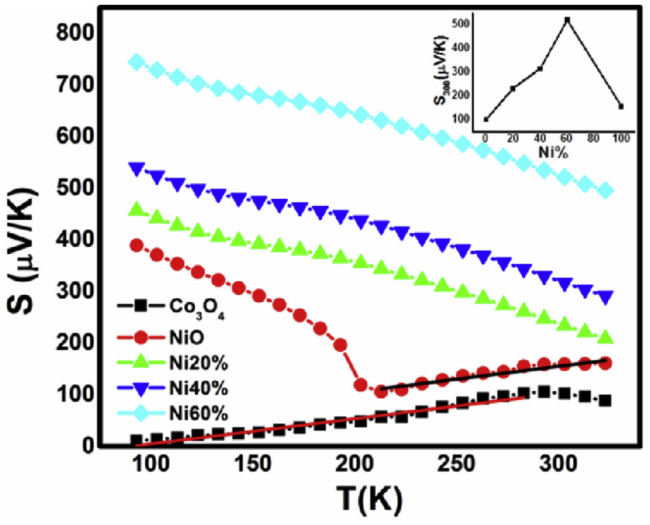

Fig. 6. S vs. T of the NPs. The linear fit of the degenerate part of the S-T plots of Co_3O_4 and NiO NPs. The inset shows the S_{300} versus Ni content of the nanoparticles.

$$S_d = \frac{k_B}{e}\left[\frac{E_f}{k_B T} + \left(r + \frac{5}{2}\right)\right] \quad (3)$$

where E_f is the Fermi energy, k_B is the Boltzmann constant, e is the electron charge and r is scattering parameter. The linear behavior of the S-1000/T plots for the Ni-Co oxides NPs (see Fig. 7) confirm their non-degenerate features and suggests a domination of the phonon diffusion contribution in the total thermopower of the samples. The slope of the S -1000/T plots illustrated in Fig. 7 allows to estimate the E_f values of the Ni-Co oxides NPs. The values were found to be nearly the same and equal to ~0.015 eV. This means that variation of the Ni content has no influence on the Fermi energy of the NPs. It is necessary to take into consideration that the estimated values are possible not very accurate because of the contribution of the S_g to the total thermopower of the samples.

The Seebeck coefficient of nominally Co_3O_4 NPs increases with the increase of the temperature (Fig. 6) which is typically a feature of degenerate semiconductor. For a degenerate semiconductor, the diffusion contribution to thermopower can be described by the following formula assuming that the material is a quasi-free electron system [29].

$$S = \frac{\pi^2 k_B^2 T}{3eE_f} \quad (4)$$

E_f value of 0.054 eV was estimated for the Co_3O_4 NPs which is comparable to the thermal energy ($2k_BT$) at room temperature confirming the degeneracy of the NPs. The S-T plot of the NiO NPs suggests a transition state from a degenerate to non-degenerate behavior at T = 283 K. $S_{(NiO)}$ decreases with the increase of temperature up to 213 K in a non-degenerate feature. Beyond this temperature, the $S_{(NiO)}$ increases suggesting a degenerate semiconductor behavior (Fig. 6). The Fermi energy E_f magnitudes were calculated from the linear fit of S-1000/T and S-T plots presented in Figs. 6 and 7 using equations (3) and (4) and were found to be 0.025 and 0.049 eV, respectively.

The inset of Fig. 6 shows the room temperature Seebeck coefficient S_{300} variation with the Ni ratio in the NPs. The results reveal that the substitution of Ni has a significant effect on the thermoelectric properties of the Co_3O_4 NPs where S_{300} increases with the increase of the Ni content. However, the pure NiO NPs have Seebeck coefficient value intermediate of those of Ni-Co oxides and pure Co_3O_4 NPs. Noteworthy, the S_{300} values of the NPs under study are in the range 100–500 μV/K. These values are relatively larger than the value of 5 μV/K reported by Windisch Jr. et al. [9] for sputter-deposited $Ni_{1-x}Co_xO_{4/3}$ thin films which can be attributed to the smaller particle size in our case.

4. Magnetic properties

4.1. AC susceptibility

To study the magnetic properties of the materials at hand, the temperature dependence of the AC susceptibility were measured at frequency 300 Hz. The AC susceptibility measurement is an important tool to characterize the small magnetic particles that exhibit spin-glass behavior, inter-particle interaction, antiferromagnetic-paramagnetic transition, superparamagnetism and other magnetic features. The magnetic susceptibility vs. temperature plots depicted in Fig. 8 show that the magnetic susceptibility increases with the increase of temperature up to a certain value T_N and then decreases in a typical antiferromagnetic-paramagnetic transition. An estimate of the Néel temperature T_N was made by extrapolating the inverse of susceptibility lines to intersect with the temperature axis. The T_N values were found to be much smaller than the reported value of the bulk materials. Indeed, it is well known that the T_N of an antiferromagnetic material is severely altered in systems of reduced dimensionality [30–33]. As the nanoparticle size approaches the magnetic correlation length of the system, the spin disorder at the nanoparticle surface spreads throughout the core of the nanoparticle, thus weakening the resultant exchange interactions and lowering the antiferromagnetic transition temperature [34]. A shift in the T_N values can be observed as the Ni content increases which may be attributed to the increase of the magnetic moment. For deep exploratory, one should take into account that the ideal bulk antiferromagnetic exhibit magnetic moment per particle equal to zero due to the complete spin compensation. However, as the particles size decreases to the nanoscale, the materials exhibit high magnetic moment due to the breaking of exchange bonds involving the surface atoms [35–37]. Consequently, spins at the surface of the nanoparticles induce uncompensated magnetic moments, deviating from the antiferromagnetic alignment. The magnetic moments of the NPs under study were calculated using the equation: $\mu_p = 2.83\sqrt{\chi_M T}$ where, T is the temperature and χ_M is the molar magnetic susceptibility. The

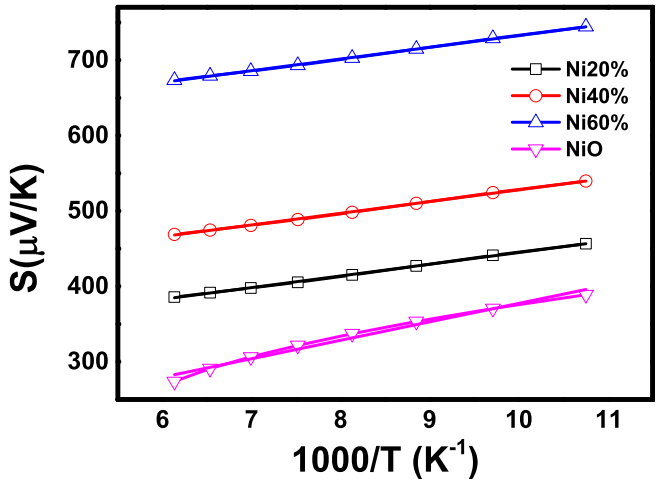

Fig. 7. S vs. 1000/T of the Ni-Co oxides NPs and the part of the non-degenerate behavior of the NiO NPs.

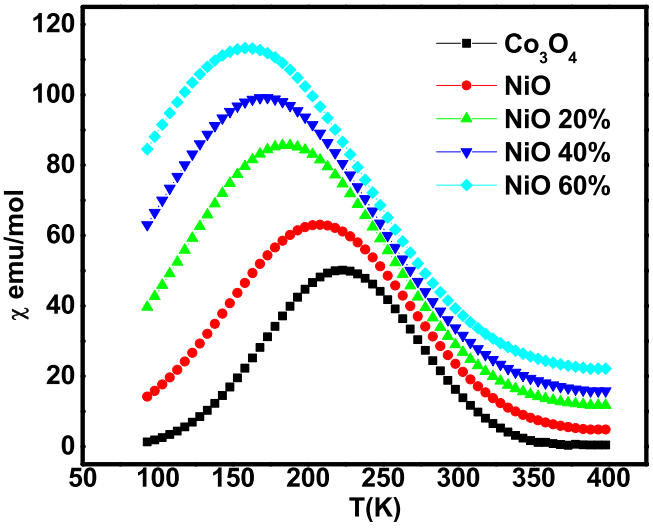

Fig. 8. AC susceptibility vs. temperature for the NPs.

determined values are tabulated in Table 1 and indicate that it is possible that the observed shift in the Néel temperatures as the Ni content increases is due to the increase of the uncompensated spins that may create a magnetic moment destabilizing the antiferromagnetic state [38].

The aforementioned results show that the Ni incorporation in the Co_3O_4 NPs has significant effect on the electrical conductivity, Seebeck coefficient and AC susceptibility values. Obviously, as the Ni content increases, the electrical conductivity decreases dramatically (coincidentally, the activation energies for conduction increase) while both of the Seebeck coefficient and the magnetic susceptibility increase. This variation results from the structural rearrangements that accompany the Ni substitution for Co sites in the Co_3O_4 lattice. Clues to specifying these structural variation are apparent from the XRD patterns of the prepared samples. As the Ni content increases to Ni60%, the spinel structure predominates without any evidence for the presence of any other phases while the XRD pattern of NiO NPs indicates to a non-spinel structure. However, for Ni-Co oxide nanoparticles where spinel structure is formed (samples of Ni content up to 60%), the Ni replaces Co at lattice sites in the spinal crystal and this is accompanied with a shift in the XRD peak, increase in the lattice parameters and decrease in the crystallite sizes. These results are coincidence with those reported by other research groups [9,39] and suggest a relationship between the increase of Ni content and a gradual loss of the spinel structural order. Noteworthy, loss of the spinel structure order is more likely if the larger Ni^{2+} ($r = 0.72$ Å) substitutes the smaller Co^{+3} ($r = 0.63$ Å) in the octahedral sites [40]. Substitution of Ni for Co exclusively at octahedral sites is almost universally accepted, based on stability considerations [41].

5. Conclusions

In conclusion, Co_3O_4, NiO and Ni-Co oxides nanoparticles have been successfully synthesized using the co-precipitation method. A study of these nanoparticles temperature-dependent dc conductivity illustrated exponential behavior confirming their semiconductive nature. The conduction mechanism of the Co_3O_4 and Ni-Co oxides nanoparticles can be explained by existence of hopping processes whether between the Ni^{2+} and/or Co^{2+} and the Co^{3+} in the octahedral site or between the octahedral and tetrahedral sites. While, the conduction in the NiO nanoparticles is attributed to the large polarons conduction mechanism. The Ni-Co oxides nanoparticles are non-degenerate semiconductive and the diffusion mechanism is dominant. In contrast, the Co_3O_4 nanoparticles show degenerate semiconductor behavior while NiO nanoparticles exhibit a transition from non-degenerate to degenerate state with the temperature variation. All the nanoparticles show typical antiferromagnetic-paramagnetic transition at Néel transition temperatures.

Acknowledgement

Financial support from Spanish Ministerio de Economía y Competitividad (MAT2013-40950-R), Gobierno del Principado de Asturias (GRUPIN14-060) and EDRF funding are acknowledged.

References

[1] J. Xiang, J.W. Lu, Y. Hu, H. Yan, C.M. Lieber, Nature 441 (2006) 489.
[2] T.W. Kim, M.A. Woo, M. Regis, K. Choi, J. Phys. Chem. Lett. 5 (2014) 2370–2374.
[3] Y. Li, W. Qiu, F. Qin, H. Fang, Hadjiev, V.G. Litvinov, D. Bao, J.J. Phys. Chem. C 120 (2001) 4511–4516.
[4] S. Selcuk, A. Selloni, J. Phys. Chem. C 119 (2015) 9973–9979.
[5] J.F. Marco, J.R. Gancedo, M. Gracia, J. Gautier, L. Ríos, E.I. Palmer, H.M. Greaves, C.F.J. Berry, J. Mater. Chem. 11 (2001) 3087.
[6] E.M.M. Ibrahim, Appl. Phys. A 89 (2007) 203–208.
[7] L.F. Hu, L. Wu, M. Liao, M.Y. Fang, X. S. Adv. Mater. 23 (2011) 1988.
[8] L. Hu, L. Wu, M. Liao, X. Hu, X. Fang, Adv. Funct. Mater. 22 (2012) 998–1004.
[9] C.F. Windisch Jr., K.F. Ferris, G.J. Exarhos, S.K. Sharma, Thin Solid Films 420 –421 (2002) 89–99.
[10] K.J. Kim, T.Y. Koh, J. Sol-Gel Technol. 77 (2016) 528–533.
[11] St.G. Christoskova, M. Stoyanova, M. Georgieva, D. Mehandjiev, Mater. Chem. Phys. 60 (1999) 39.
[12] F. Svegl, B. Orel, I. Grabec-Svegl, V. Kaucic, Electrochim. Acta 45 (2000) 4359.
[13] E.M.M. Ibrahim, S. Hampel, A.U.B. Wolter, Kath, M. El-Gendy, A.A. Klingeler, R. Täschner, C. Khavrus, V.O. Gemming, T. Leonhardt, A.B. Büchner, J. Phys. Chem. C 22509 (2012) 116.
[14] A. Naveen, N.S. Selladurai, Electrochimica Acta 173 (2015) 290–301.
[15] L.C. Schumacher, I.B. Holzhueter, I.R. Hill, M. Dignam, J. Electrochim. Acta 6 (1990) 975.
[16] P.M.S. Monk, S. Ayub, Solid State Ionics 99 (1997) 115.
[17] P.N. keng, G. Poillerat, J.F. Koenig, P. Chartier, B. Lefez, J. Lopitaux, M. Lenglet, J.Electrochem. Soc. 1777 (1995) 142.
[18] N.J. Tharayil, R. Raveendran, A. Vaidyan, Mater. Sci.Res. India 4 (2007) 69–75.
[19] E.M.M. Ibrahim, S.A. Saleh, A.M.A. Hakeem, J. Alloys Compd. 429 (2007) 19–24.
[20] S.A. Arrhenius, Über die Dissociationswärme und den Einflusß der Temperatur auf den Dissociationsgrad der Elektrolyte, Z. Phys. Chem. 4 (1889) 96–116.
[21] S. Krupichka, Physics of Ferrite and Related Magnetic Oxides, second ed., Mir, Moscow, 1976.
[22] F.J. Morin, T.H. Gebella, Phys. Rev. 93 (1970) 433.
[23] N.F. Mott, E.A. Davis, Electronic Process in Non-crystalline Materials, Clarendon Press, 1979. UK.
[24] D. Adler, Feinleib, J. Phys. Rev. 112 (1970) 2–3.
[25] M.Th. Makhlouf, B.M. Abu-Zied, T.H. Mansoure, Adv. Powder. Tech. 25 (2014) 560–566.
[26] S.A. Makhlouf, M.A. Kassem, M.A. Abdel-Rahim, J. Mater. Sci. 44 (2009) 3438–3444.
[27] Teuku Muhammad Roffi, Kazuo Uchid, Shinji Nozaki, J. Cryst. Growth 414 (2015) 123–129.
[28] G.S. Nolas, J. Sharp, H.J. Goldsmid, Thermoelectrics Basic Principles and New Materials Developments, vol. 45, Springer Series in Materials Science, Heidelberg, Germany, 2001.
[29] H.J. Trodahl, Phys. Rev. B 51 (1995) 6175.
[30] E.M.M. Ibrahim, Silke Hampel, Raghunandan Kamsanipally, Juergen Thomas, Kati Erdmann, Susanne Fuessel, Christine Taeschner, Vyacheslav O. Khavrus, Thomas Gemming, Albrecht Leonhardt, Bernd Buechner, Carbon 63 (2013) 358–366.
[31] E.M.M. Ibrahim, J. Appl. Phys. 113 (2013) 154301.
[32] M. Tadic, D. Nikolic, G.R. MatjazPanjan, G.R. Blake, J. Alloys Compd. 647 (2015) 1061–1068.
[33] G.A. Babu, G. Ravi, Y. Hayakawa, Appl. Phys.A 119 (2015) 219–232.
[34] Natalia Rinaldi-Montes, Pedro Gorria, David Martínez-Blanco, Antonio B. Fuertes, Inés Puente-Orench, Luca Olivi, Jesús A. Blanco, AIP Adv. 6 (056104) (2016).
[35] S.K. Sharma, J.M. Vargas, E.D. Biasi, F. Beron, M. Knobel, K.R. Pirota, C.T. Menases, S. Kumar, C.G. Lee, P.G. Pagliuso, C. Rettori, Nanotechnology 21 (2010) 035602.
[36] Marin Tadic, Dobrica Nikolic, Matjaz Panjan, Graeme R. Blake, J. Alloys Compd. 647 (2015) 1061–1068.
[37] Tony Jaumann, E.M.M. Ibrahim, Silke Hampel, Diana Maier, Albrecht Leonhardt, Bernd Büchner, Chem. Vap. Depos. 17 (2013) 1–7.
[38] A.K. Sarfraz, S.K. Hasanain, Acta Phys. Pol. A 125 (2014) 139–144.
[39] Y.E. Roginskaya, O.V. Morozova, E.N. Lubnin, Y.E. Ulitina, G.V. Lopukhova, S. Trasatti, Langmuir 13 (1997) 4621.
[40] J.A. Dean (Ed.), Lange's Handbook of Chemistry, thirteenth ed., McGraw-Hill, NY, 1985, pp. 3–121.
[41] W.J. King, A.C.C. Tseung, Electrochim. Acta 19 (1974) 493.